Zeitschrift für Physikalische Chemie, Bd. 201, S. 137–150 (1997)

Jahn-Teller Effect of Cu^{2+} in II–VI Compounds*

By P. Thurian, R. Heitz, G. Kaczmarczyk, A. Hoffmann, I. Broser

TU-Berlin Institut für Festkörperphysik, Hardenbergstr. 36, D-10623 Berlin, Germany,
Tel. ++49-30-31422476, Fax: ++49-30-31422064,
email: thurian@physik.TU-berlin.DE

T. Telahun, C. Schrepel, C. Goebel and U. Scherz

TU-Berlin, Institut für Theoretische Physik, Hardenbergstr. 36, D-10623 Berlin, Germany

(Received August 24, 1996)

CdS / ZnS / Copper / Photoluminescence / Local vibrational modes

High-resolution spectroscopy of weakly Cu-doped CdS and polymorphic ZnS crystals leads to the detection of new Cu^{2+} ($^2E - {}^2T_2$) zero-phonon lines which have been investigated as a function of temperature and in magnetic fields up to 15 T. As a result, an unique termscheme for Cu^{2+} in the sulfide host compounds is presented. We interpret the observed Cu^{2+} transitions in ZnS and CdS crystals by a moderate Jahn-Teller coupling of the electronic states to a local vibrational mode of E symmetry and a Huang-Rhys factor of S = 0.8 for ZnS and S = 1.1 for CdS. We report on parameter-free calculations of the magnetic-field splitting of Cu^{2+} centers in II–VI compounds, which show a general agreement with the observed spectra. For ZnS:Cu^{2+} the agreement between the calculated and observed g values is excellent, whereas some differences for the $^2T_2$ ground-state g factors occur. This is due to the neglect of the T_2 mode coupling in the Jahn-Teller calculation. The local vibrational modes of copper in ZnS and CdS are investigated and fitted in a cluster calculation using the valence-force model of Kane including Coulomb forces. An E mode at 32.4 meV is found to be the dominant coupling mode in ZnS whereas a T_2 mode at 21.3 meV is obtained for CdS.

1. Introduction

The copper defect is one of the most prominent impurities in II–VI compounds [1–4]. It gives rise to various luminescence and absorption bands in the visible and near infrared spectral region. The Cu^{2+} defect is of special interest, because a maximum of information has been compiled so far experimentally and theoretically for the Cu^{2+}($^2E - {}^2T_2$)-transitions, which makes

* Presented at the 13th International Symposium on Electrons and Vibrations in Solids and Finite Systems (Jahn-Teller Effect) Berlin 1996.

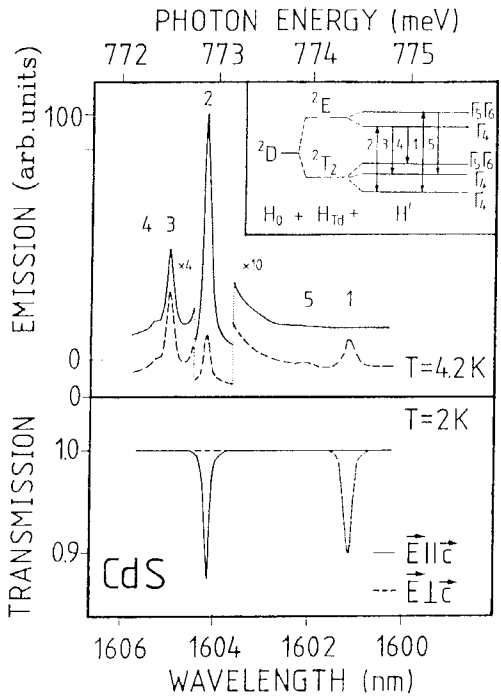

Fig. 1. Zero-phonon line region of the Cu^{2+} ($^2E - {}^2T_2$) transition in CdS. The solid line of the emission spectrum (top) is taken at a temperature of $T = 2$ K, and that in broken line at $T = 4.2$ K. The solid line of the transmission spectrum refers to a polarization parallel and the broken line perpendicular to the c-axis.

it a favored example to study the mechanisms determing the optical spectra of transition metal impurities. Interpretations of these spectra, using simple models for the Jahn-Teller effect, were discussed controversially up to now [5–13] and especially the Zeeman behavior was not understood sufficiently. The aim of this paper is to present an unique experimental and theoretical description of the Cu^{2+} centers in CdS and ZnS including crystal field theory and electron-phonon interaction. The simplicity of the d^9 system allows the investigation of the Jahn-Teller effect on the fine-structure of the defect without the difficulties of the electron–electron interaction which is important for the d^2-d^8 systems.

2. Experimental results

Most of the CdS and ZnS single crystals are grown by the Broser-Warminski method [14], and are subsequently doped in the ppm region by diffusion of copper. The CdS crystals are pure wurtzite crystals, whereas ZnS crystals

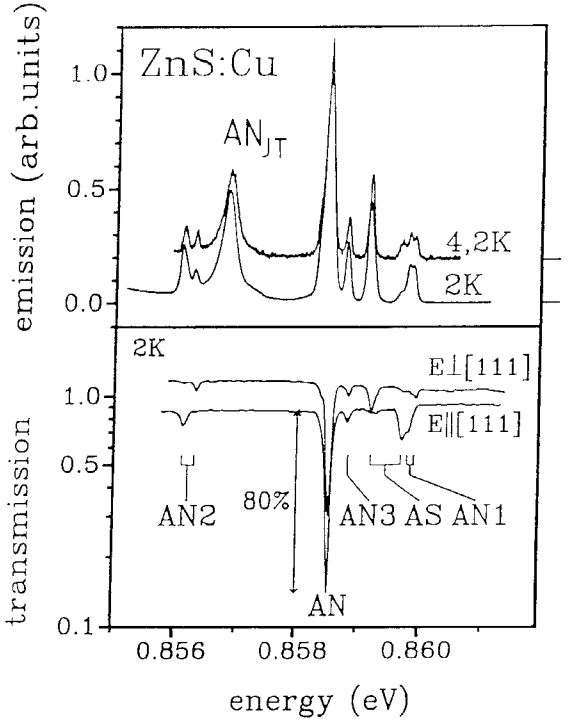

Fig. 2. Zero-phonon line region of the Cu^{2+} ($^2E - {}^2T_2$) transition in polymorphic ZnS. The main lines AN, seen in emission (top) and transmission (bottom) are attributed to the cubic centers. The other lines AN1, AN2, AN3, and AS originate from Cu^{2+} centers in different polytypes. The emission spectrum is shown at different temperatures. The transmission spectrum is given for polarization perpendicular and parallel to the c axis.

are preferably cubic with a polytypic contribution in the order of 10−20%. Some crystals with higher Cu concentration (100−3000 ppm) are grown by the Brigman method. The Cu^{2+} ion substitutes the cation, and is located in first order in a tetrahedrally coordinated S^{2-} environment in both materials. In CdS and in noncubic ZnS the tetrahedron is slightly distorted, and a small trigonal distortion has to be taken into account. In the case of CdS the nearest-neighbor sulfur ion along the c axis is closer, whereas it is farther away in wurtzite ZnS compared with the other three nearest-neighbor sulfur ions.

All polytypic modifications of ZnS consist of sequences of Zn−S layers being stacked along the [111] direction of growth. Thus four different lattice sites exist for a substitutional impurity if the possible arrangements of the Zn−S layers above and below the two layers, which contain the impurity and their ligands, are considered. The four sites are called AN (cubic), (AS,

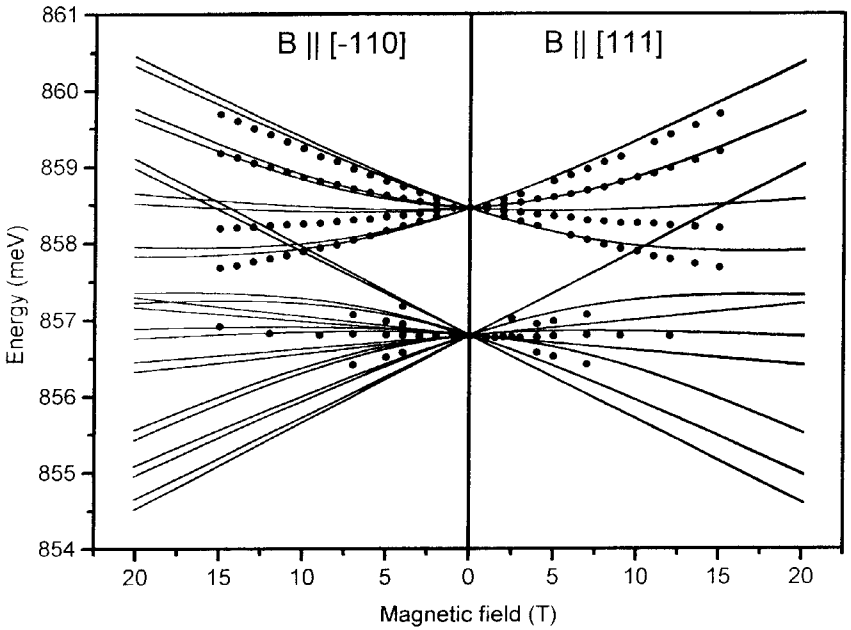

Fig. 3. Zeeman-pattern of the Cu^{2+} AN center in ZnS. Comparison of the transitions between the $\Gamma_8(^2E)$ excited state quartet and the ground-state $\Gamma_7(^2T_2)$ doublet (higher lines) and the ground state $\Gamma_8(^2T_2)$ quartet (lower lines) with the observed Zeeman pattern (points) of the AN center in ZnS. All calculated lines are included.

PN) (axially distorted), and PS (hexagonal). The latter P indicates a prismatic, A an antiprismatic coordination, S the existence of a single third-neighbor on the stacking axis, and N its absence [15]. In this contribution we consider six Zn−S layers, which lead to a classification scheme of 16 different lattice sites for the substitutional Cu^{2+} impurity [16].

The tenfold degeneracy of the ^2D multiplet of the Cu^{2+} ion, having a $3d^9$ configuration, is lifted by a tetrahedral crystal field (*Td* symmetry) into a $^2T_2$ ground-state and a ^2E excited state multiplet. The spin-orbit interaction further splits the $^2T_2$ ground-state into a lower Γ_7 doublet and a higher Γ_8 quartet of the symmetry double group. A trigonal crystal field of C_{3v} symmetry, caused by the wurtzite crystal structure or stacking faults, splits the Γ_8 energy levels into a Γ_4 doublet and a $\Gamma_{56} = \Gamma_5, \Gamma_6$ Kramers doublet. The Γ_7 state becomes a Γ_4 state.

The high-resolution emission and transmission experiments are performed with a 0.75 m double-grating monochromator (Spex) and a cooled germanium detector (North Coast). For the luminescence experiments the crystals are excited with the blue lines of an Ar^+-ion laser in the charge-transfer band of the Cu^{2+} center. A detailed investigation of the Cu^{2+} exci-

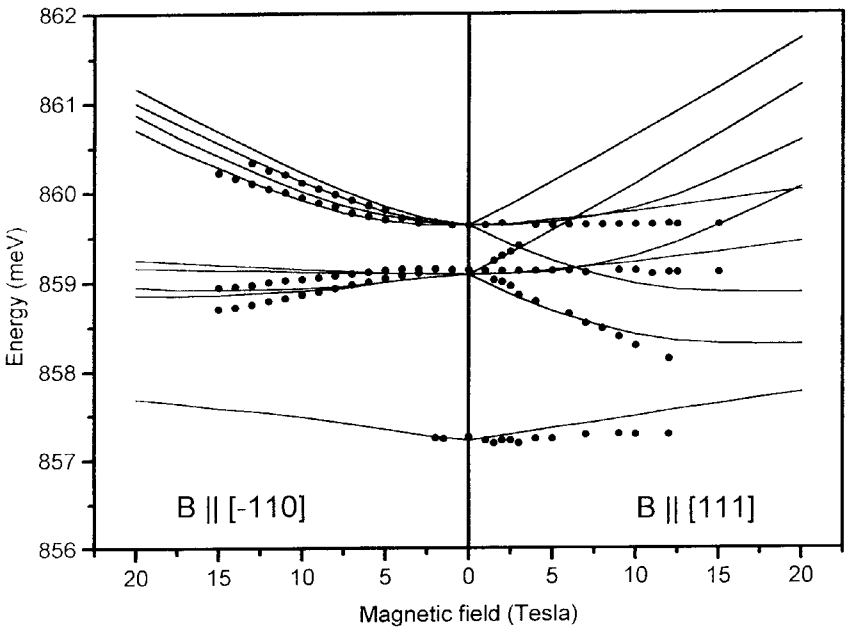

Fig. 4. Zeeman-pattern of the Cu^{2+} AS center in ZnS. Shown are the transitions between the split $\Gamma_{5,6}(^2E)$ excited state Kramers doublet (highest lines) and $\Gamma_4(^2E)$ excited state doublet (middle lines) and the lowest $\Gamma_8(^2T_2)$ ground-state doublet. The lowest transition is between the $\Gamma_4(^2E)$ excited state doublet and $\Gamma_{5,6}(^2T_2)$ doublet level. The points denote the observed Zeeman lines.

tation mechanism in II–VI compounds is described in Ref. [17]. Here we focus our attention on the fine-structure of the intercenter Cu^{2+} ($^2E - {}^2T_2$) transition.

Cu^{2+} in CdS

The zero-phonon line (ZPL) region of the Cu^{2+} emission and transmission is shown in Fig. 1. The energy differences between emission lines 2, 3, and 4 determine the threefold splitting of the $^2T_2$ ground state. The twofold splitting of the excited ^2E state is represented through the energy differences between the lines 1 and 2. Thus five Kramers doublets of the Cu^{2+} center in CdS are identified, and their relative energies listed in Table 4.

Cu^{2+} in ZnS

Highly resolved Cu^{2+} emission and absorption spectra in ZnS are shown in Fig. 2. Twelve different Cu^{2+} centers in the polymorphic ZnS crystal have been identified experimentally, but here we concentrate on those for which Zeeman data are available.

Table 1. Fitted parameters for the Cu^{2+} centers in ZnS polytypes and CdS. AN denote the cubic and AN1, AN2, AS and PN trigonal centers in ZnS. All energies are given in meV.

	AN	AN1	AN2	AS	PN	CdS
Dq	75.51	75.85	75.38	75.51	74.07	64.77
D_0	0	1.87	2.51	−2.06	15.82	10.04
K	0	9.97	9.99	10.02	9.98	−24.86
K'	0	1.37	1.39	1.39	1.38	−2.49
ζ_{Td}	−73.47	−73.01	−73.52	−73.53	−73.50	−69.35
ζ'_{Td}	−90.72	−90.72	−91.47	−90.89	−90.81	−76.60
$\zeta_{C_{3v}}$	0	8.08	6.22	−3.10	−7.15	−3.25
$\zeta'_{C_{3v}}$	0	8.03	6.16	−3.10	9.20	−1.71
$\hbar\omega$	32.46	32.36	32.58	32.71	32.29	33.72
E_{JT}	26.44	24.90	25.12	26.15	26.16	36.50
S	0.81	0.77	0.77	0.80	0.81	1.1

Table 2. Comparison of the g factors observed for the cubic AN center of Cu^{2+} in ZnS with the calculated values. The g factors are given for magnetic fields between $B = 8$ T and $B = 15$ T. The zero-field energies are obtained from the fitting procedure and are given in meV.

Center	Multiplet	Energy	$g_{\|[1\bar{1}0]}^{\text{theor}}$	$g_{\|[1\bar{1}0]}^{\text{exp}}$	$g_{[111]}^{\text{theor}}$	$g_{[111]}^{\text{exp}}$
AN	$\Gamma_8(^2E)$	858.46	1.68	1.69±0.01	1.57	1.67±0.01
			1.45		1.54	
	$\Gamma_8(^2T_2)$	1.68	1.06	0.96±0.15	1.08	0.96±0.15
			2.28		2.25	
	$\Gamma_7(^2T_2)$	0.00	0.59	0.61±0.02	0.60	0.62±0.02

Cubic center AN

The unpolarized ZPLs of the cubic AN center are shown in Fig. 2. The main line, detected in emission and absorption, is attributed to the $\Gamma_8(^2E) - \Gamma_7(^2T_2)$ transition. The unpolarized ZPL at 856.78 meV is attributed to the $\Gamma_8(^2E) - \Gamma_8(^2T_2)$ transition of the AN center.

Axial centers AN1, AN2, AS, and PN

The axial Cu^{2+} centers in ZnS exhibit a twofold splitting of the excited ^2E state. The assignment of the different ZPLs to the corresponding defect centers, and the corresponding ^2E splitting, are shown in Fig. 2. We observe a zero-field splitting of 0.08, 0.20 and 0.51 meV for the AN1, AN2, and

Table 3. Comparison of the observed g factors for $\mathbf{B}\perp\mathbf{c}$ and $\mathbf{B}\|\mathbf{c}$ of the axial centers AN1, AN2, and AS of Cu^{2+} in ZnS with the calculated values. The two theoretical g factors in brackets refer to the smallest and largest difference between the four energy levels of the ^2E quartet, the mean value of which has been observed. The magnetic field dependent g factors are compared at the same field B as observed.

Multiplet	Energy	$g_\perp^{theor}$	$g_\perp^{exp}$	$g_\|^{theor}$	$g_\|^{exp}$
			AN1		
$\Gamma_{56}(^2E)$	859.87	$\bar{g} = 1.47$	1.49±0.08[a]	1.68	1.53±0.08
$\Gamma_4(^2E)$	859.77	{1.34, 1.60}[a]		1.65	1.53±0.08
$\Gamma_4(^2T_2)$	2.26	1.0		0.85	
$\Gamma_{56}(^2T_2)$	1.94	0.80		2.13	
$\Gamma_4(^2T_2)$	0.00	0.64	0.56±.05	0.93	0.79±.05
			AN2		
$\Gamma_{56}(^2E)$	856.25	1.61[a]	1.67±.02[a]	1.65	1.51±.04
$\Gamma_4(^2E)$	856.04	1.34*		1.61	1.51±.04
$\Gamma_4(^2T_2)$	2.25	0.99		0.98	
$\Gamma_{56}(^2T_2)$	1.96	0.84		2.18	
$\Gamma_4(^2T_2)$	0.00	0.53	0.41±.05	1.06	0.97±.09
			AS		
$\Gamma_4(^2E)$	859.62	1.61[a]	1.64±.02[a]	1.52	1.45±.02
$\Gamma_{56}(^2E)$	859.07	1.53[a]		1.47	1.45±.02
$\Gamma_4(^2T_2)$	2.00	0.74		1.31	
$\Gamma_{56}(^2T_2)$	1.88	1.20		2.45	
$\Gamma_4(^2T_2)$	0.00	0.34	0.29±.02	1.41	1.45±.02

[a] Derived by taking zero-field splitting and term interaction into account, see Eq. (1).

Table 4. Comparison of the observed g factors of Cu^{2+} in CdS with the calculated values. The experimental and theoretical g values have been deduced for magnetic fields between 7 T and 15 T. Energies are given in meV.

Multiplet	Energy	$g_\perp^{theor}$	$g_\perp^{exp}$	$g_\|^{theor}$	$g_\|^{exp}$
$\Gamma_{56}(^2E)$	774.40	0.01	0.00±.05	1.56	1.55±.02
$\Gamma_4(^2E)$	772.88	0.16	0.09±.03	1.55	1.55±.02
$\Gamma_{56}(^2T_2)$	0.56	0.05		2.23	1.70±.10
$\Gamma_4(^2T_2)$	0.41	1.72	1.15±.05	2.29	1.87±.02
$\Gamma_4(^2T_2)$	0.00	0.46	0.13±.03	2.35	1.93±.02

AS centers, respectively. In comparison with these axial centers the magnitude of the zero-field splitting for the PN center is increased to 2.45 meV. It should be mentioned that the sign of the ^{2}E splitting parameter is the same for the PN, AN1, and AN2 centers, whereas for the AS center a reversed sign is observed. The energetic positions with respect to the ground state are given in Table 3.

Thus, it can be summarized that the $^2T_2$ ground-state splitting of Cu^{2+} is strongly quenched compared to the free-ion value. This is due to covalent bonding and a Jahn-Teller effect, which is discussed in the next section. Furthermore, no $^{63/65}$Cu isotope shift has been resolved, giving us an upper limit of 10 μeV/nucleon for Cu^{2+} in the sulfide-host compounds. Since only a local vibrational mode of T_2 symmetry may cause an isotope shift, such a mode is unlikely and we restricted the calculation to an E mode in first order.

3. Theoretical model and comparison with the experiment

The Hamiltonian of static crystal-field theory has been extended to include the Jahn-Teller coupling of an E mode to the electronic ^{2}D multiplet. The optical spectra between the excited ^{2}E and the $^2T_2$ ground-state multiplets are described by the crystal-field parameter Dq, the higher order trigonal spin-orbit coupling parameter D_0 of the ^{2}E multiplet, the trigonal crystal-field parameters K and K' for the $^2T_2$ multiplet and for the $^2T_2 - {}^2$E term interaction respectively, the corresponding tetrahedral and trigonal spin-orbit coupling parameters ζ_{Td}, ζ'_{Td}, $\zeta_{C_{3v}}$, and $\zeta'_{C_{3v}}$, the energy of the local vibrational mode $\hbar\omega$, and the Jahn-Teller energy $E_{JT} = S\hbar\omega$, where S denotes the Huang-Rhys factor. Our numerical method of coupling to oscillator functions enabled us to take up to 14 excited energy levels into account. The automatic fitting procedure, using evolution strategy resulted in the parameters compiled in Table 2 for various copper centers in ZnS and CdS. The values of Dq and the spin−orbit coupling parameters are not far from those of earlier fittings in terms of crystal-field theory [2, 18]. The energy of the local vibrational mode is practically the same for all the different copper centers in ZnS.

Magnetic field splitting

The Hamiltonian depends linearly on the magnetic field. The orbital reduction factor, describing covalent bonding effects, has been set equal to the ratio of the spin-orbit coupling parameter of the copper centers and of the free ion value. As a result, the magnetic field splitting has been calculated without any additional fitting parameters and is therefore a test of the fine-structure fit. The nonlinear magnetic field splitting $\Delta E(B)$ results from

the repulsion of nearby energy levels having the same symmetry and is described by a g factor, which may alternatively be independent of B or depending on B according to

$$g\mu_B B = [\Delta E^2(B) - \Delta E^2(0)] \quad (1) \qquad \text{or} \qquad g(B)\mu_B B = |\Delta E(B)|$$

where μ_B denotes the Bohr magneton and B the magnetic field. The g factors depend on the direction of the magnetic field with respect to the crystallographic axes [111] or [−110] and the results for the cubic AN center in ZnS is given in Table 2. The comparison between the calculated energy-level differences and the observed Zeeman pattern of the AN center is shown in Fig. 4. We included all possible transitions between the calculated energy levels of the excited ^2E and the $^2T_2$ ground-state multiplet. The calculated and observed g factors are compiled for some of the trigonal copper centers in polytypic ZnS in Table 3. The zero-field energies in column two are obtained from the fine-structure fit. The direct comparison of the observed transitions with the calculated energy-level differences for the trigonal AS center is shown in Fig. 3. The calculated splittings of the three doublets $\Gamma_4(^2T_2)$ ground state, $\Gamma_{56}(^2T_2)$, and $\Gamma_4(^2T_2)$ show a nonlinear behavior in the $\mathbf{B} \perp \mathbf{c}$ configuration for all the trigonal centers in ZnS. Compared to the AN center the Zeeman pattern is more anisotropic. This is mainly due to the anisotropic splitting of the excited ^2E state. The calculation shows a strong nonlinear behavior for small magnetic fields below $B = 5$ T as a consequence of the energy levels having the same symmetry.

The observed emission lines of $CdS:Cu^{2+}$ between the excited ^2E and the $^2T_2$ ground states split approximately linear with the magnetic field above $B = 7$ T [10] and the corresponding g factors, taken in the region $7 < B < 15$ T, are shown in Table 4 for B perpendicular and parallel to the c-axis. The general nonlinear behavior of the splittings is reproduced by the calculation. In order to compare the theoretical results with the observed splittings it is necessary to determine the symmetry of the initial and final state of the various transitions from the polarization of the observed lines and the selection rules. This had been done with the help of the calculated splittings and the comparison between the observed and calculated g factors is shown in Table 4. The calculated g factors of the excited state doublets $\Gamma_4(^2E)$ and $\Gamma_{56}(^2E)$ agree well with the observation, whereas there are some discrepancies between the observed and calculated g factors of the three doublets in the $^2T_2$ ground state. This is a striking difference to the situation in ZnS. In order to clarify this question we investigated the local vibrational properties of copper in ZnS and CdS.

Local vibrational properties

The energy of the local vibrational E mode, which was introduced in the Jahn-Teller fit of the experimental data, was observed experimentally in

ZnS in the vibronic emission and absorption sideband of the Cu^{2+} ($^2T_2 - {}^2E$) transition at 32.4 meV. For CdS only the vibronic sideband of the Cu^{2+} ($^2E - {}^2T_2$) emission is observed. The superposition of vibronic emissions and local vibration phonon modes make a clear distinction difficult for CdS. However, the peak structures at 21.4 meV and 24.6 meV were tentatively attributed to local vibrational modes (LVMs) of the copper center.

In order to get insight into the local vibrational system of copper in ZnS and CdS we performed calculations using a valence-force model. The interatomic forces of cubic and hexagonal semiconductors had been parametrized in consideration of symmetry requirements by Keating [19]. The simple model for bond stretching and bond bending forces was extended by Kane [20] to include up to third nearest neighbor interactions. He demonstrated that the phonon dispersion curves of various crystals can be interpreted by a small number of parameters including an effective atomic charge to take the long-range Coulomb interaction into account. We used this model to set up the dynamical matrix, the eigenvalues of which are the squares of the vibration frequencies. In order to apply the Keating-Kane model to the calculation of LVMs at point defects in semiconductors we used a cluster of 281 vibration atoms around the defect in ZnS and 295 atoms around the defects in CdS and ZnO. The vibration frequencies were obtained from a numerical diagonalization of the dynamical matrix. The localization of the vibrational mode is determined from the vibration amplitudes as obtained from the corresponding components of the eigenvector of the dynamical matrix. We selected the local vibrational modes by the condition that the sum of the squared components of the eigenvector corresponding to the atoms in the first three shells is larger than 0.3. We adopted the scaling-factor approximation (SFA) [21] to describe the change of the interatomic forces in the vicinity of the defect. The scaling factor s is defined by $p_d = p + sp$, where p is the bond stretching or bond bending valence-force parameter of the perfect crystal and p_d the corresponding parameter at the defect. The scaling factor was fitted to obtain the observed energy of the LVM.

ZnS: Cu

LVMs are expected to occur mainly in the energy region, where the phonon density of the perfect crystal is low. For ZnS, the gap in the calculated phonon density of states between the acoustic and optical phonon band lies between 27.1 meV and 32.8 meV.

No Raman data about LVMs of copper was published up to now. Choosing the scaling factor of $s = -0.3$, we obtain the best agreement of the calculation with the observed 32.4 meV mode in ZnS. This vibrational

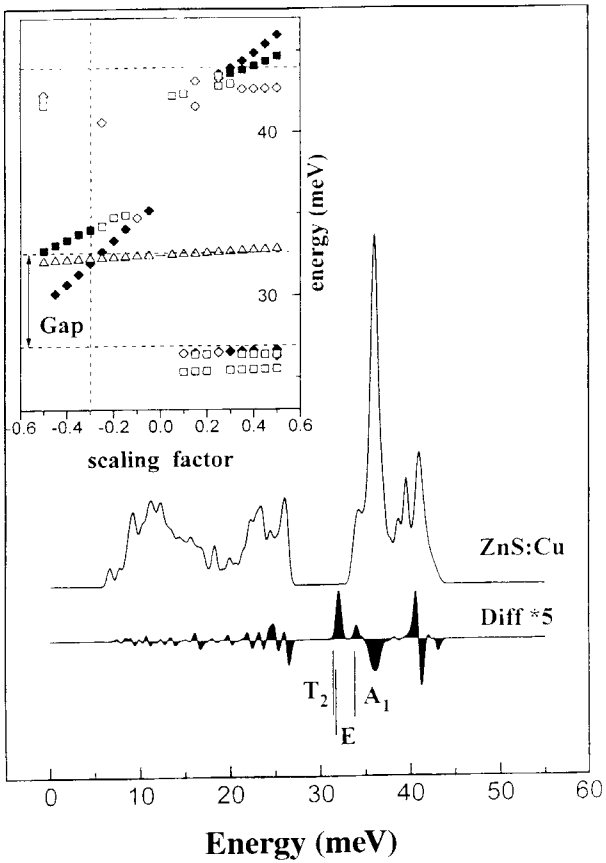

Fig. 5. Calculated phonon density of states for ZnS:Cu for a scaling factor of $s = -0.3$. The difference between ZnS and ZnS:Cu is shown. The insert gives the energy position of the local vibrational modes as a function of the scaling factor.

mode with E symmetry at 32.3 meV is mainly localized at the impurity and its nearest sulfur ligands. Fig. 5 represents the density of phonon states of the perfect cubic ZnS crystal (full line) and the change due to the Cu impurity for a scaling factor of −0.3. The insert shows the energy shift of the LVMs as a function of the scaling factor. Due to hybridization the localization of a LVM decreases with the scaling factor when its energy is shifted from regions of low density of phonon states into regions of high density of phonon states of the perfect crystal and vice versa. This explains the delocalization of the modes and their localization when crossing an energy region of host modes by changing the scaling factor.

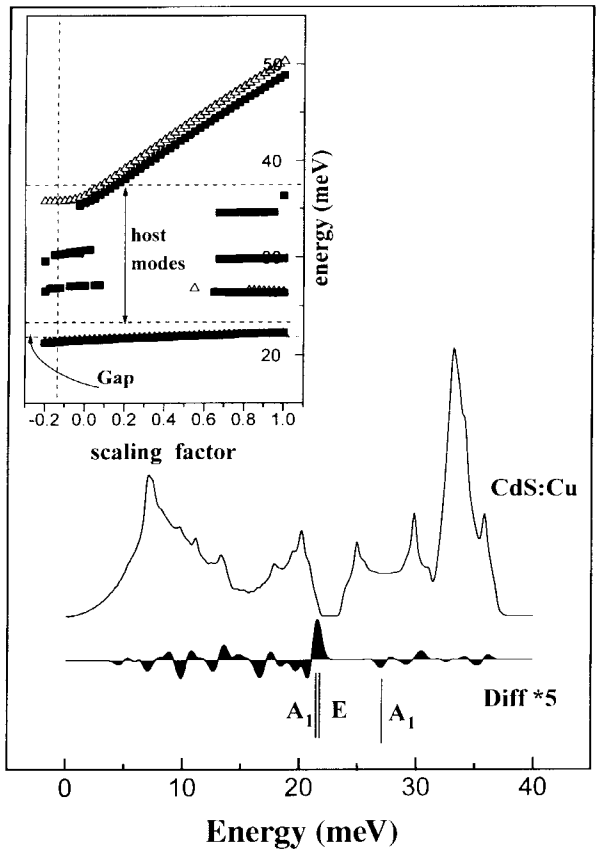

Fig. 6. Calculated phonon density of states for CdS:Cu for a scaling factor of $s = -0.125$. The difference between CdS and CdS:Cu is also shown. The insert gives the energy position of the local vibrational modes as a function of the scaling factor.

Additionally to the E mode at 32.3 meV further modes (A_1 at 34.0 meV, T_2 at 32.0 meV) are obtained by the calculation.

CdS:Cu

In contrast to ZnS, the acoustical phonon band as well as the optical phonon band of the perfect crystal are shifted to lower energies in CdS. The gap in the phonon density of states occurs between 22 meV and 24 meV. For each scaling factor, a A_1 mode at 21.3 meV and an E mode at 21.4 meV are obtained in the calculation. These modes correspond to a T_2 mode in zincblende symmetry. Choosing a scaling factor of $s = -0.125$ we were

able to fit the other observed peaks in the vibronic emission sideband of $CdS:Cu^{2+}$. Further modes at 26.85 meV (A_1) and 35.8 meV (E) were found in the calculation.

The difference in the local vibrational properties of the copper center in ZnS and CdS is thus directly correlated with the phonon density of states of the perfect crystal and the hybridization of the local vibrational copper modes. The LVM E mode in ZnS is hybridized with the host modes in CdS, whereas the A_1 and E modes at 21 meV in CdS are hybridized with the host modes in ZnS.

This has important consequences for the validity of the Jahn-Teller calculations using only E modes in the fitting procedure. For ZnS, the fit parameter of the phonon energy (see Table 1) of 32.4 meV agrees with the energy of the LVM of copper, confirming the realistic fit of this parameter. For CdS, the restriction to an E mode seems to be insufficient in the context of this results. For a better fit of the Zeeman behavior of the $^2T_2$-ground state $T_2 = E \times A_1$ modes have to be taken into account. Usually, the coupling to additional modes reduces the g-factors. The difference between the observed and calculated g values is in the order of 0.3, whereas generally larger g values are obtained in the calculation than in the observed spectra.

4. Conclusion

We presented a detailed experimental and theoretical study of the Cu^{2+} transition in ZnS and CdS. The observed fine structure is similar for the axial Cu^{2+} centers in CdS and polytypic ZnS. A splitting of the excited ^2E state and an anisotropic Zeeman behavior was obtained. The observed fine structure was fitted by a Jahn-Teller coupling to E modes only. The parameter-free calculation of the Zeeman behavior reproduces the Zeeman pattern and the nonlinearities caused by the term interaction for both ZnS and CdS. The quantitative agreement between the fit and the experimental data was excellent in the case of ZnS, whereas differences in the Zeeman behavior of the $^2T_2$ ground state in CdS occur. These differences are mainly caused by the change of the behavior of the local vibrations at copper in ZnS and CdS. Whereas the E mode coupling is sufficient in the case of ZnS, coupling to a second LVM with T_2 symmetry should be taken into account. However, it should be pointed out that the simple coupling to an E mode explains the fine structure and the general Zeeman behavior of the Cu^{2+} centers in both ZnS and CdS.

References

1. H. A. Weakliem, J. Chem. Phys. **36** (1962) 2117.
2. I. Broser, H. Maier and H.-J. Schulz, Phys. Rev. **140** (1965) A2135.
3. R. E. Dietz, H. Kamimura, M. D. Sturge and A. Yariv, Phys. Rev. **132** (1963) 1559.

4. A. Suzuki and S. Shionoya, J. Phys. Soc. Japan **31** (1971) 1455.
5. B. Clerjaud and A. Gelineau, Phys. Rev. **B9** (1974) 2832.
6. H. Maier and U. Scherz, Phys. Status Solidi **B62** (1974) 153.
7. T. Yamaguchi and H. Kamimura, J. Phys. Soc. Jpn. **33** (1972) 953.
8. V. Z. Polinger, S. I. Boldyrev, Phys. Status Solidi (b) **137** (1986) 241.
9. B. Clerjaud, Acta Phys. Polonica 6, Vol. **A73** (1988) 909.
10. I. Broser, A. Hoffmann, R. Heitz and P. Thurian, J. Lumin. **48 and 49** (1991) 693.
11. P. Thurian, R. Heitz, T. Jentzsch, A. Hoffmann and I. Broser, Physica **B185** (1993) 239.
12. T. Telahun, P. Thurian, A. Hoffmann, I. Broser and U. Scherz, Mater. Sci. Forum **196–201** (1995) 767.
13. T. Telahun, U. Scherz, P. Thurian, R. Heitz, A. Hoffmann and I. Broser, Phys. Rev. **B53** (1996) 1274.
14. I. Broser and R. Broser-Warminsky, Dtsch. Patentamt, Patent No. 814 (1950) 193.
15. T. Buch, B. Clerjaud, B. Lambert and P. Kovacs, Phys. Rev. **B7** (1973) 184.
16. U. W. Pohl, A. Ostermaier, W. Busse and H.-E. Gumlich, Phys. Rev. **B42** (1990) 5751.
17. R. Heitz, A. Hoffmann, P. Thurian and I. Broser, J. Phys. **C4** (1992) 157.
18. U. Scherz, J. Phys. Chem. Solids **30** (1969) 2077.
19. P. N. Keating, Phys. Rev. **145** (1966) 637.
20. E. O. Kane, Phys. Rev. **B31** (1985) 7865.
21. R. M. Feenstra, R. J. Hauenstein and T. C. McGill, Phys. Rev. **B28** (1983) 5793.